HHS Public Access

Author manuscript

Acta Acust United Acust. Author manuscript; available in PMC 2019 April 09.

Published in final edited form as:

Acta Acust United Acust. 2018 ; 104(5): 874–877. doi:10.3813/AAA.919236.

Auditory brainstem response wave III is correlated with extracellular field potentials from nucleus laminaris of the barn owl

Paula T. Kuokkanen[1], **Anna Kraemer**[2], **Richard Kempter**[1], **Christine Köppl**[3], and **Catherine E. Carr**[2]

[1)]Department of Biology, Institute for Theoretical Biology, Humboldt-Universitätzu Berlin, Philippstr 13, 10115 Berlin, Germany. paula.kuokkanen@hu-berlin.de

[2)]Department of Biology, University of Maryland, College Park MD 20742, USA.

[3)]Department of Neuroscience, Carl von Ossietzky University, 26109 Oldenburg, Germany.

Summary

The auditory brainstem response (ABR) is generated in the auditory brainstem by local current sources, which also give rise to extracellular field potentials (EFPs). The origins of both the ABR and the EFP are not well understood. We have recently found that EFPs, especially their dipole behavior, may be dominated by the branching patterns and the activity of axonal terminal zones [1]. To test the hypothesis that axons also shape the ABR, we used the well-described barn owl early auditory system. We recorded the ABR and a series of EFPs between the brain surface and nucleus laminaris (NL) in response to binaural clicks. The ABR and the EFP within and around NL are correlated. Together, our data suggest that axonal dipoles within the barn owl nucleus laminaris contribute to the ABR wave III.

Introduction

The auditory brainstem response (ABR) is a complex signal comprised of several waves [2]. Despite decades of research, no uniform model on the origin of the ABR has emerged. ABRs are related to the extracellular field potentials (EFPs) that can be recorded within the brainstem nuclei. Important for a connection between ABR and EFP is the dipole behavior of EFPs, which may originate from the branching patterns and the activity of axons [1] and/or the distribution of synaptic inputs onto dendritic arbors [3, 4, 5]. Axonal sources are typically discounted in EEG models because their contributions are assumed to be negligible far from their sources due to their assumed quadrupole behavior. In the auditory brainstem, however, dipolar EFPs may be dominated by axonal terminal zones because of the very high temporal precision of neuronal signals in the sub-millisecond range [1]. This recent insight about the strong contribution of axonal branching patterns to far-field dipoles suggests a revision of earlier models of the ABR [6].

To test the hypothesis that axons shape the ABR, we used the barn owl circuit where we have extensive knowledge of the connectome and the physiological delays between, and properties of, different nuclei. The nuclei are large and geometrically simple, which may

allow separation of the neural elements that cause far-field potentials. We recorded these sources with both microelectrodes and ABR electrodes [7, 8]. Although the analysis of multi-site recordings is theoretically a powerful tool to constrain EFP and ABR models, the separation and identification of sources is generally not possible, because most systems contain multiple cell types and synaptic inputs. These complications affected the level of explanation in otherwise rigorous pioneering studies of sources of the ABR in the cat [9, 10].

We hypothesize that the axonal dipoles within the barn owl NL provide a major contribution to the ABR wave III [11]. To test this hypothesis, we combined ABR and EFP recordings in response to binaural clicks, and compared voltage waveforms, power spectral densities, and coherence.

Methods

Experimental Paradigms

Experiments were conducted at the University of Maryland using 3 adult American barn owls *Tyto furcata.* Electrophysiological recording procedures were identical with [12], and more details about the ABR recording procedures can be found in [13]. All procedures conformed to NIH Guidelines for Animal Research and were approved by the University of Maryland IACUC. Anaesthesia was induced for two owls by intramuscular injections of 10–16 mg/kg ketamine hydrochloride and 3 mg/kg xylazine. Supplementary doses were administered to maintain a suitable plane of anaesthesia. For one owl, anesthesia was induced by 1.6 g/kg urethane i.m. Body temperature was maintained at 39°C by a feedback-controlled heating blanket[12]. Recordings were made in a sound-attenuating chamber (IAC Acoustics, New York, NY).

Tungsten electrode (EFP) recordings.—Tungsten electrodes with impedances between 2 and 20 MΩ were used for extracellular recordings. Signals were amplified, and line noise removed with a HumBug (Quest Scientific, North Vancouver, BC, Canada). To control for effects of this filter, we made recordings with and without it and compared the spectra. We found changes at harmonics of 60 Hz, but frequencies > 350 Hz were not significantly affected. Signals were band-pass filtered and digitized (DD1, TDT). Acoustic stimuli were digitally generated, presented dichotically and calibrated. At a given recording site, we measured iso-level frequency response curves to pure tones and then tuning to ITD. In all experiments, voltage responses were recorded with a sampling frequency of 48,077 Hz, and saved for off-line analysis. For each recording location, we played binaural zero-ITD click stimuli of 50 to 300 repetitions, at 50 and 70 dB SPL.

ABR recordings.—For ABR recordings, platinum subdermal needle electrodes (Grass F-E2; West Warwick, RI) were placed at the vertex of the skull (active) and in the neck muscle at the midline (reference). To combine tungsten electrode and ABR recordings, the skull was vented, and the active electrode was placed in the bone layers of the mediorostral edge of the craniotomy above the brain, near the mid-line. Conductivity gel (Spectra 360) was placed on the electrodes for better conductance. The differential signal was recorded using a WPI

DAM-50 amplifier (0.1–10,000 Hz) World Precision Instruments, Sarasota, FL), and the same stimuli as above.

Data analysis

For both EFP and ABR recordings, we used the following procedures to analyze the data: For each click, the voltage trace from the stimulus onset to 80 ms after the onset was analyzed. All the data analysis was done with Matlab 9.0 (MathWorks, Natick, MA). The response traces were averaged over all repetitions of the stimulus presentation (50 – 300 repetitions). We then identified local extrema in the ABR by the zero-crossings of the first derivative of the voltage trace.

We further analyzed the spectral characteristics of the responses. Because of the short duration of the click responses (10 ms), we enhanced the frequency resolution (to 1 Hz) by concatenating all responses to one long trace after calculating a running average over 20 trials. This yielded a better signal-to-noise ratio than concatenating the original trials but preserved e.g. possible fluctuations over recording time. We applied a periodic hamming window of 10 ms to decrease 100 Hz harmonics (due to concatenation of 10 ms responses) and after calculating the power spectral density and coherence, we removed remaining harmonic peaks by replacing the value at each (n·100±[0,2]) Hz bin ranges by the average of the neighboring values at bins ($n \cdot 100$) ± [3, 20] Hz.

The coherence measures the correlations between signals over spectral frequencies, normalized by the autocorrelation of the reference signal. Coherence ranged from 0 – 1, where 0 means no coherence between the signals and 1 means that signals were fully coherent. We calculated the coherence of the pre-processed traces with respect to the ABR with the MATLAB implementation ‘mscohere’ which uses the Welch’s averaged modified periodogram method.

Results

The ABR reflects the summed responses to sound by brainstem neural centers, and consists of a series of waves, with a clear succession of peaks across the auditory brainstem. It shows three prominent positive peaks within the first 5 ms of stimulation (Fig. 1), designated as waves II, III and IV. Waves II and III are separated by a prominent negative peak (N2) [11]. The shortest-latency peak (wave I) appears only at high levels (about > 60dB SPL for clicks). We predicted that axonal sources entering NL would generate a dipole-like response to clicks, dominated by frequencies < 2 kHz, that would be detected by an electrode in the brain near NL [1]. We tested this prediction with recordings between the brain surface and NL using click stimuli. Recordings were made at 1 mm intervals, starting adjacent to the active ABR electrode, and penetrating through the cerebellum into the brainstem and adjacent to NL (Fig. 1). Furthermore, we determined the power spectral densities (PSDs) of the ABR and the EFP responses (Fig. 2A), and compared them with ABRs. Because sources contributing at different frequencies and located at different depths might decay with distance in a frequency-dependent manner, we also calculated the coherence between the ABR and the brainstem field potentials (Fig. 2B).

Temporal coincidence of binaural ABR and NL responses.

The pronounced peak at 2.8 ms delay in the field potential at the depth of NL (adjacent to NL) was well visible in the ABR (wave III; Fig. 1). A peak with a similar latency but of much smaller amplitude is also visible in recordings at the depth of the cerebellum. Within lower cerebellum (about 4 – 8 mm), there was also a spatially wide peak coinciding with ABR peak IV at 3.8 ms delay.

Similar spectral densities of the ABR and field potentials.

Typically, power spectral densities (PSDs) had a large peak 100 – 500 Hz which then fell off with increasing frequency. The PSDs of recordings adjacent to NL (~ 9 – 11 mm) and the PSD of the ABR showed a shoulder at ~ 1 kHz. These peaks were less visible at other depths (Fig. 2A), except at 5 mm. The $1/f$ scaling of the spectral power is a general property of the EFPs [3].

Coherence of the ABR with field potentials.

The coherence of the field potential of the tungsten electrode at the cerebellar surface (adjacent to ABR electrode, depth 0.5 mm) with the ABR was typically low (< 0.3) for 50 dB stimulation at frequencies < 700 Hz (Fig. 2B). The coherence was highest (0.5) at ~ 1 kHz, and at > 2 kHz the coherence was low. For 70 dB SPL stimulation the coherence was moderate to high (> 0.8) at 0 – 7 kHz (not shown).

Through the cerebellum (0.5 – 8 mm depth), the coherence of the EFP with the ABR varied from low to moderate (0 – 0.6) at frequencies 100 – 1500 Hz, with a typical peak at ~ 1 kHz, and was low beyond 2 kHz for 50 dB SPL stimulus amplitude (Fig. 2B). For 70 dB SPL the coherence peaked typically at ~ 1 kHz, ~ 2 kHz, and at 5 – 8 mm at ~ 4 kHz, but was low (< 0.4) at frequencies < 1 kHz and > 5 kHz (not shown).

Through the brainstem (8 – 10 mm depth), the coherence of the EFP with the ABR was moderate to high (0.5 – 0.9) at frequencies 100 – 1500 Hz for 50 dB SPL (Fig. 2B) and low at higher frequencies > 1.5 kHz. For 70 dB SPL the coherence peaked (0.7 – 1) at ~ 1 kHz, ~ 2 kHz and ~ 4 kHz, but was low (< 0.4) at frequencies < 1 kHz (not shown).

Below NL (depth 11 mm) there was a high plateau (0.7 – 1) in the coherence with the ABR at 200 – 1500 Hz for 50 dB SPL. For 70 dB SPL the coherence was high at < 500 Hz (0.5 – 0.8), and peaked at ~ 2 kHz and at ~ 4 kHz (0.7 – 0.9).

Discussion

Here we show that the timing of the wave III of the ABR coincides with the peak in the field potential that can be observed around NL (Fig. 1). We hypothesize that large dipoles can be created in the auditory brainstem by axonal projections connecting the nuclei. Such a dipole surrounds NL and originates with the input axons from NM that branch and terminate extensively within NL [1]. The polarity reversal of this dipole may only be observed for monaural stimulation. The dipole has been predicted to have a spectral peak at ~ 1 kHz, which we observed around NL for the binaural click stimuli. Furthermore we see a consistent, large peak at ~ 1 kHz in the coherence between the ABR and the EFP around

NL. Our findings are consistent with the hypothesized dipole-like field around NL. Whether similar structures exist within or between other nuclei and other species remains to be determined. In cat inferior colliculus the axonal tracts have been suggested to contribute to the wave IV [14].

In other model systems such as cats and guinea pigs, the synaptic dipole in medial and lateral olivary nuclei could be far reaching [9, 10, 6, 8]. Such synaptic dipoles have not been observed in the barn owl NL. By contrast, we have recently shown that the field created around individual NL neurons is weak and decays fast, not making a large contribution to the EFP even locally within NL [15].

Conclusion.

In barn owls, wave III of the ABR coincided with a peak in the EFP at the depth of NL. Around NL, the PSDs revealed peaks around ~ 1 kHz both for the ABR and for the EFP. Furthermore, the coherence of the ABR and EFPs also showed a peak at ~ 1 kHz at all recording depths. More research is needed to determine whether wave III of the ABR derives from activity within NL, the output of NL, or other correlated sources.

Acknowledgement

We gratefully acknowledge the assistance of G. Ashida, L. Kettler, and N. Thiele. Supported by NSF CRCNS IOS1516357, NIH DC00436, and NIH P30 DC0466 to the University of Maryland Center for the Evolutionary Biology of Hearing, the Bundesministerium für Bildung und Forschung (BMBF): German – US-American collaboration “Field Potentials in the Auditory System” as part of the NSF/NIH/ANR/BMBF/BSF CRCNS program, 01GQ1505A and 01GQ1505B.

References

[1]. McColgan T, Liu J, Kuokkanen PT, Carr CE, Wagner H, and Kempter R. Dipolar extracellular potentials generated by axonal projections. eLife, 6:e26106, 2017. [PubMed: 28871959]

[2]. Huang C-M and Buchwald JS. Factors that affect the amplitudes and latencies of the vertex short latency acoustic responses in the cat. Electroencephalogr. Clin. Neurophysiol., 44:179–186, 1978.

[3]. Buzsáki G, Anastassiou CA, and Koch C. The origin of extracellular fields and currents — EEG, ECoG, LFP and spikes. Nat. Rev. Neurosci, 13:407–420, 2012. [PubMed: 22595786]

[4]. Goldwyn JH, Mc Laughlin M, Verschooten E, Joris PX, and Rinzel J. Signatures of somatic inhibition and dendritic excitation in auditory brainstem field potentials. J. Neurosci, 37:10451–10467, 2017. [PubMed: 28947575]

[5]. Bédard C, Kröger Hand Destexhe A. Modeling extracellular field potentials and the frequency-filtering properties of extracellular space. Biophys. J, 86:1829–1842, 2004. [PubMed: 14990509]

[6]. Ungan P, Yağcioğlu S, and Özmen B. Interaural delay-dependent changes in the binaural difference potential in cat auditory brainstem response: implications about the origin of the binaural interaction component 1. Hear. Res, 106:66–82, 1997. [PubMed: 9112107]

[7]. Saunders JC, Coles RB, and Gates GR. The development of auditory evoked responses in the cochlea and cochlear nuclei of the chick. Brain Res, 63:59–74, 1973. [PubMed: 4764322]

[8]. Brittan-Powell EF, Dooling RJ, and Gleich O. Auditory brainstem responses in adult budgerigars (melopsittacus undulatus). J. Acoust. Soc. Am, 112:999–1008, 2002. [PubMed: 12243189]

[9]. Achor LJ and Starr A. Auditory brain stem responses in the cat. I. intracranial and extracranial recordings. Electroencephalogr. Clin. Neurophysiol, 48:154–173, 1980. [PubMed: 6153332]

[10]. Melcher JR and Kiang NYS. Generators of the brainstem auditory evoked potential in cat. III: identified cell populations. Hear. Res, 93:52–71, 1996. [PubMed: 8735068]

[11]. Palanca-Castan N, Laumen G, Reed D, and Köppl C. The binaural interaction component in barn owl (tyto alba) presents few differences to mammalian data. J. Assoc. Res. Otolaryngol, 17:577–589, 2016. [PubMed: 27562803]

[12]. Carr CE, Shah S, McColgan T, Ashida G, Kuokkanen PT, Brill S, Kempter R, and Wagner H. Maps of interaural delay in the owl's nucleus laminaris. J. Neurophysiol, 114:1862–1873, 2015. [PubMed: 26224776]

[13]. Kraemer A, Baxter C, Hendrix A, and Carr CE. Development of auditory sensitivity in the barn owl. J. Comp. Physiol. A, 203:843–853, 2017.

[14]. Land R, Burghard A, and Kral A. The contribution of inferior colliculus activity to the auditory brainstem response (ABR) in mice. Hear. Res, 341:109–118, 2016. [PubMed: 27562195]

[15]. Kuokkanen PT, Ashida G, Kraemer A, McColgan T, Funabiki K, Wagner H, Köppl C, Carr CE, and Kempter R. Contribution of action potentials to the extracellular field potential in the nucleus laminaris of barn owl. J. Neurophysiol, 119(4):1422–1436, 2018. [PubMed: 29357463]

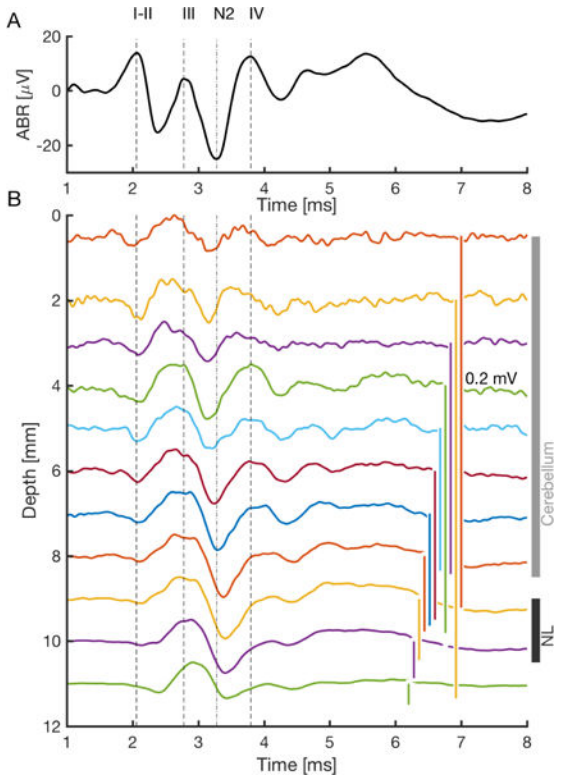

Figure 1:

Average waveforms (50 – 300 repetitions) of binaural ABR and EFP responses. **A**: Auditory brainstem response (ABR) to 50 dB SPL clicks. **B**: EFP (depths 0.5 –11 mm) across the cerebellum (vertical grey bar) and the auditory brainstem (depths next to NL indicated by black bar). The electrode was adjacent to, but not within NL. **A–B:** Stimulus onset is at time zero. Vertical dashed lines mark the peaks of the ABR waves I-II, III, and IV, respectively. The vertical dash-dotted line marks the second negative peak N2.

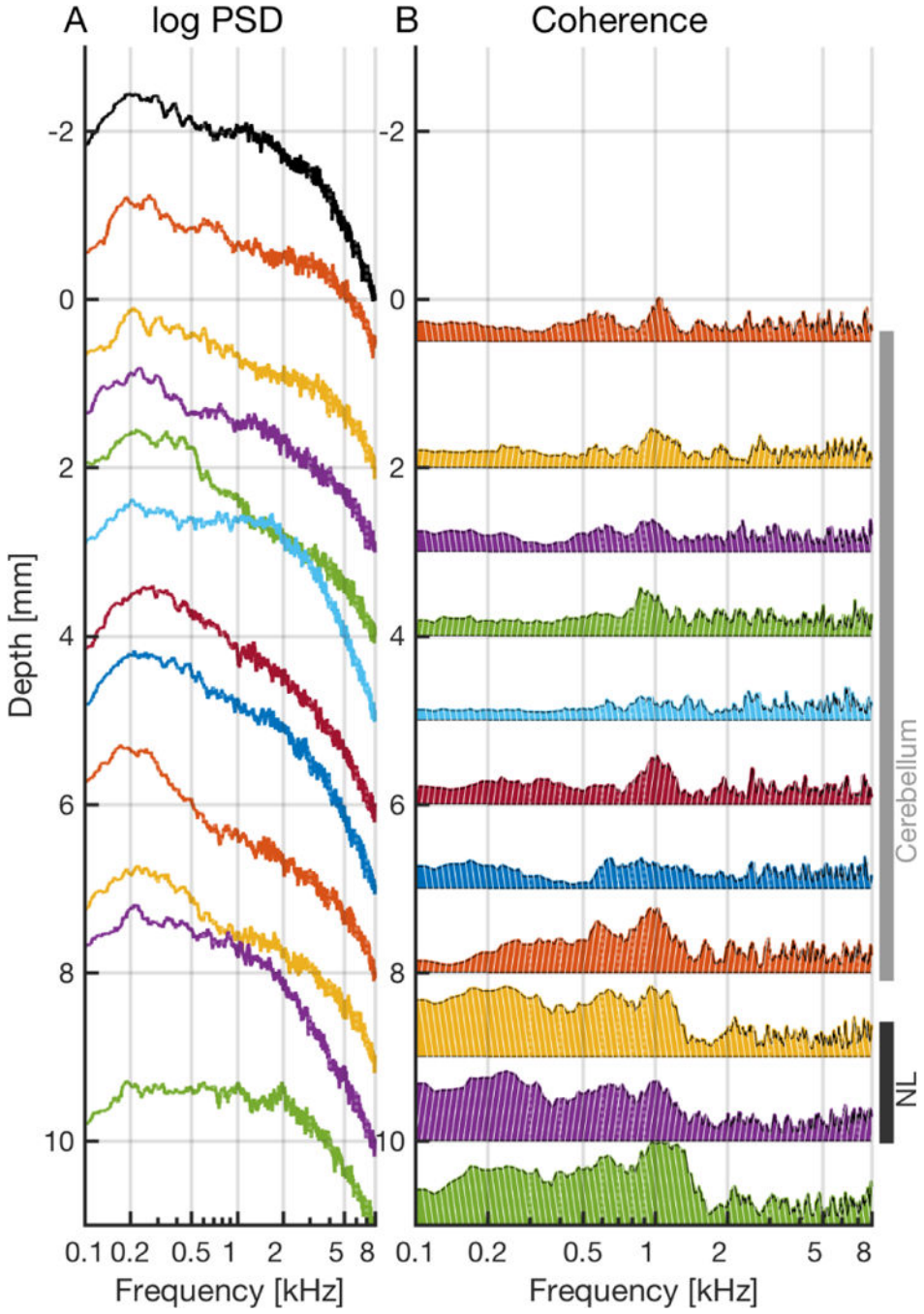

Figure 2:

Spectral characteristics of the ABR and EFP. A: Power spectral density (PSD) (in log scale) of the ABR (black) and field potentials (colors). One mm in depth corresponds to one order of magnitude in PSD. The value of each log(PSD)-curve at 8 kHz corresponds to the respective depth of the recording. B: Coherence of the field potentials with respect to the ABR. Depth of one millimeter corresponds to coherence of one. Each coherence is filled

from the baseline of zero upwards, and zero is located at the respective depth of the recording. A–B: Stimulus amplitude: 50 dB SPL.